DIGITAL ACCESS TO SCHOLARSHIP AT HARVARD
DASH.HARVARD.EDU

HARVARD LIBRARY
Office for Scholarly Communication

Interferon Regulatory Factor 3 Is Regulated by a Dual Phosphorylation-dependent Switch

Citation

Panne, Daniel, Sarah M. McWhirter, Tom Maniatis, and Stephen C. Harrison. 2007. "Interferon Regulatory Factor 3 Is Regulated by a Dual Phosphorylation-Dependent Switch." Journal of Biological Chemistry 282 (31): 22816–22. doi:10.1074/jbc.M703019200.

Permanent link

http://nrs.harvard.edu/urn-3:HUL.InstRepos:41542802

Terms of Use

This article was downloaded from Harvard University's DASH repository, and is made available under the terms and conditions applicable to Other Posted Material, as set forth at http://nrs.harvard.edu/urn-3:HUL.InstRepos:dash.current.terms-of-use#LAA

Share Your Story

The Harvard community has made this article openly available.
Please share how this access benefits you. Submit a story .

Accessibility

THE JOURNAL OF BIOLOGICAL CHEMISTRY VOL. 282, NO. 31, pp. 22816–22822, August 3, 2007
© 2007 by The American Society for Biochemistry and Molecular Biology, Inc. Printed in the U.S.A.

Interferon Regulatory Factor 3 Is Regulated by a Dual Phosphorylation-dependent Switch*◆

Received for publication, April 10, 2007, and in revised form, May 23, 2007 Published, JBC Papers in Press, May 25, 2007, DOI 10.1074/jbc.M703019200

Daniel Panne[‡], Sarah M. McWhirter[§1], Tom Maniatis[§], and Stephen C. Harrison[‡2]

From the [‡]Department of Biological Chemistry and Molecular Pharmacology, Howard Hughes Medical Institute, Harvard Medical School, Boston, Massachusetts 02115 and [§]Department of Molecular and Cellular Biology, Harvard University, Cambridge, Massachusetts 02138

The transcription factor interferon regulatory factor 3 (IRF-3) regulates genes in the innate immune response. IRF-3 is activated through phosphorylation by the kinases IKKε and/or TBK1. Phosphorylation results in IRF-3 dimerization and removal of an autoinhibitory structure to allow interaction with the coactivators CBP/p300. The precise role of the different phosphorylation sites has remained controversial. Using purified proteins we show that TBK1 can directly phosphorylate full-length IRF-3 *in vitro*. Phosphorylation at residues in site 2 (Ser[396]—Ser[405]) alleviates autoinhibition to allow interaction with CBP (CREB-binding protein) and facilitates phosphorylation at site 1 (Ser[385] or Ser[386]). Phosphorylation at site 1 is, in turn, required for IRF-3 dimerization. The data support a two-step phosphorylation model for IRF-3 activation mediated by TBK1.

The transcription factor IRF-3[3] is a central component of the innate immune system. It is required for expression of type I interferons α and β (IFN-α and IFN-β), the chemokine RANTES (regulated on activation normal T cell expressed and secreted), and many other genes that respond to viral and bacterial infection (1–4). In the absence of infection, IRF-3 is in a latent conformation in the cytoplasm (1, 5). Upon infection, the host detects an invading pathogen through pattern recognition receptors such as the toll-like receptors or the cytoplasmic receptors RIG-I and Mda-5. Depending on the microbial pathogen, distinct signaling pathways are triggered, many of which lead to activation of IRF-3. IRF-3 is activated by phosphorylation mediated directly or as part of a signaling cascade by the IκB kinase (IKK)-related kinases, TBK1 and IKKε (6–10). Phosphorylation of IRF-3 leads to dimerization, translocation to the nucleus, and association with the coactivator CREB-binding protein (CBP) or the closely related p300 (1, 11–13).

IRF-3 shares a conserved N-terminal DNA-binding domain with other members of the interferon response factor family of transcription factors (14). It also contains a C-terminal IRF association domain (IAD), which mediates phosphorylation-dependent homo- or hetero-oligomerization with other IRF family members and interaction with CBP/p300 (15). The crystal structure of the N-terminal DNA-binding domain bound to the interferon-β promoter and the crystal structure of the IAD have been determined (14–16). Activation of IRF-3 requires phosphorylation on a cluster of serine and threonine residues in the C-terminal region of the IAD spanning amino acids 385 to 405. Despite considerable efforts, using mutagenesis, phosphopeptide mapping, and phospho-specific antibodies, the exact position and role of phosphorylation sites in the 385–405 region remain controversial. On the one hand, Fujita and co-workers (17) suggest that phosphorylation at Ser[385]/Ser[386] (site 1) is key to the activation of IRF-3 and that phosphorylation at site 2, spanning residues 396 to 405, has an auxiliary but not essential role. This view is supported by the observation that mutation of Ser[385] or Ser[386] to Ala abolishes IRF-3 activity (5, 12). In addition, Fujita and co-workers (16, 17) used a phosphospecific antibody against Ser[386] to show that overexpressed IRF-3, activated by virus or by overexpression of upstream regulators, is phosphorylated on Ser[386] and that phosphorylation on Ser[386] is observed in the dimeric form of IRF-3. On the other hand, Hiscott and colleagues (11) argue that phosphorylation of site 2 residues may also be critical for virus-inducible IRF-3 activation. For instance, substitutions of the site 2 residues Ser[396], Ser[398], Ser[402], Thr[404], and Ser[405] with the phosphomimetic Asp or Glu (IRF-3 5E) lead to a constitutive phenotype (11). Further mutagenesis and use of a phospho-specific antibody has identified Ser[396] as a key site 2 residue that is phosphorylated *in vivo* upon virus infection (18). Substitution of Ser[385] and Ser[386] with either Ala or Asp inhibits IRF-3 activation (5). Taken together, these data point to a phosphorylation-dependent mechanism of IRF-3 activation that requires serine 386 and a cluster of serine/threonine residues between Ser[396] and Ser[405].

Analysis of the crystal structure of the IAD by Qin *et al.* (15) suggested that phosphorylation of the site 2 residues 396–405 results in unfolding of an N-and C-terminal autoinhibitory structure, essentially consistent with the functional studies of Hiscott and colleagues (5, 18). Unfolding of the autoinhibitory structure by introduction of a negative charge, through either phosphorylation or mutagenesis, exposes a hydrophobic surface for interaction with CBP/p300. Qin *et al.* (15) also sug-

* The costs of publication of this article were defrayed in part by the payment of page charges. This article must therefore be hereby marked "*advertisement*" in accordance with 18 U.S.C. Section 1734 solely to indicate this fact.
◆ This article was selected as a Paper of the Week.
[1] Present address: Dept. of Molecular and Cell Biology, University of California, Berkeley, 415 Life Sciences Addition, Berkeley, CA 94720.
[2] To whom correspondence should be addressed. Tel.: 617-432-5607; Fax: 617-432-5600; E-mail: harrison@crystal.harvard.edu.
[3] The abbreviations used are: IRF, interferon regulatory factor; IBiD, interferon-binding domain; CREB, cAMP-response element-binding protein; CBP, CREB-binding protein; IAD, IRF association domain; DTT, dithiothreitol; MOPS, 4-morpholinepropanesulfonic acid; TBK1, Tank-binding kinase 1.

Downloaded from http://www.jbc.org/ by guest on October 12, 2019

gested that the dimer in the asymmetric unit of the crystal was not physiologically relevant and that the phosphorylated, rearranged C-terminal tail might be involved in subunit dimerization. In contrast, Takahasi *et al.* (16) doubt the existence of the N- and C-terminal autoinhibitory structure and interpret their crystallographic results to be consistent with the functional studies of Fujita and co-workers (12). They suggest that the dimer in the asymmetric unit is physiologically relevant and that phosphorylation of Ser^{385}/Ser^{386} results directly in IAD dimerization. Dimerization would generate a combined surface for recognition of CBP/p300 (16). This latter model was recently ruled out by a co-complex crystal structure of the IAD with the interferon-binding domain (IBiD) of CBP (19). This structure shows that removal of the autoinhibitory N and C termini of the IAD leads to exposure of a binding pocket that interacts with IBiD and that the IAD and IBiD form a 1:1 complex.

To clarify the role of phosphorylation in IRF-3 activation, as well as the role of TBK1 in this process, we purified to homogeneity full-length IRF-3, the constitutive mutant IRF-3 5E, and the kinase TBK1. We found that, as predicted, purified IRF-3 is a monomer in solution and that IRF-3 5E is a dimer. Access to highly purified and homogeneous protein preparations allowed us to map the phosphorylation sites in more detail. Monomeric IRF-3 is phosphorylated neither at site 1 nor at site 2. Dimeric IRF-3 5E is fully phosphorylated at site 1 (Ser^{385} or Ser^{386}) as a result of constitutive *in vivo* phosphorylation by an insect cell kinase. TBK1 can directly phosphorylate IRF-3, resulting in a distribution of monomeric and dimeric IRF-3, consistent with earlier findings (5, 20). Mapping of the phosphorylation sites in a purified TBK1-phosphorylated IRF-3 dimer showed 100% phosphorylation of one serine residue at site 1 (Ser^{385} or Ser^{386}) and of one serine/threonine residue at site 2 (Thr^{404} or Ser^{405}). The purified TBK1-phosphorylated IRF-3 monomer is not phosphorylated at site 1; it is fully phosphorylated on one serine at site 2 (Thr^{404} or Ser^{405}), but mutation of residues 404 and 405 to Ala does not completely abolish *in vitro* phosphorylation of site 2 residues. We also show that CBP binding requires phosphorylation at site 2, the residues of which are functionally redundant. Thus, modification in site 2 is critical for alleviating autoinhibition, for allowing interaction with CBP, and for facilitating phosphorylation at site 1. Phosphorylation at site 1 leads in turn to IRF-3 dimerization as proposed previously (17).

EXPERIMENTAL PROCEDURES

Insect Cell Culture and Baculovirus Cultivation—The recombinant baculoviruses were propagated in Sf21 insect cells with Hinks TMN-FH insect cell medium (JRH Biosciences) supplemented with 10% fetal bovine serum (JRH Biosciences). Virus titration, amplification, and storage were performed as described previously. For production of recombinant IRF-3 and IRF-3 5E, Sf21 insect cells were infected with recombinant baculovirus at a multiplicity of infection of 2.0, maintained in spinner flasks at 28 °C, and harvested by centrifugation at 64 h postinfection. For production of TBK1, Hi5 insect cells were infected with recombinant baculovirus and otherwise treated as described above.

Purification of Full-length IRF-3 and IRF-3 5E from Insect Cells—Recombinant baculovirus-infected cell pellets were lysed by freezing and then thawed in equilibration buffer containing 20 mM HEPES (pH 7.5), 500 mM NaCl, 1 mM EDTA, 1 mM phenylmethylsulfonyl fluoride, and 0.5% Nonidet P-40. For TBK1 purification, frozen cell pellets were thawed and resuspended in 20 mM HEPES (pH 7.5), 500 mM NaCl, 0.5 mM sodium fluoride, 1 mM EDTA, 0.1% Tween 20, and Complete protease inhibitors (Roche Applied Science). The cells were homogenized by sonication and the lysate clarified by centrifugation at 180,000 × *g* for 40 min. The clarified insect cell lysate was incubated with pre-equilibrated Anti-FLAG M2-agarose affinity gel (Sigma) for 1 h and then applied to a 25-ml Econo column (Bio-Rad). The resin was washed with 200 ml of equilibration buffer, and then bound protein was eluted using 0.1 mg/ml triple FLAG peptide (sequence, MDYKDHDADYKDHDIDYKDDDDK) dissolved in equilibration buffer.

Fractions were concentrated using a Centricon-plus 30 ultrafiltration unit (Amicon, Inc.) and further purified on a Hi-Load 16/60 Superdex 200 gel filtration column (GE Healthcare) equilibrated in 20 mM HEPES (pH 7.5), 150 mM NaCl, 1 mM dithiothreitol (DTT). The final protein was concentrated to 40 mg/ml for IRF-3, 14 mg/ml for IRF-3 5E, and 2.5 mg/ml for TBK1 in a Centricon-plus 30 ultrafiltration unit; aliquots were flash-frozen in liquid N_2 and stored at −80 °C. Protein concentrations were determined by diluting the sample in 10 mM KH_2PO_4 (pH 6.8), 6 M guanidine HCL and measuring the absorbance at 280 nm using a molar extinction coefficient calculated from the amino acid sequence.

IRF-3 Phosphorylation with TBK1—600 pmol of IRF-3 was incubated for 30 min at 30 °C with 24 pmol of TBK1 in a buffer consisting of 20 mM HEPES (pH 7.6), 50 mM NaCl, 20 mM β-glycerol phosphate, 1 mM sodium vanadate, 10 mM $MgCl_2$, 1 mM DTT, and 1 mM ATP.

Analytical Gel Filtration—IRF-3, IRF-3 5E, and IRF-3 phosphorylated by TBK1 were further analyzed, on a Superdex 200 10/300 gel filtration column (GE Healthcare) equilibrated in 20 mM HEPES (pH 7.5), 150 mM NaCl, and 1 mM DTT. The column was calibrated using a set of globular protein standards consisting of thyroglobulin (670 kDa), γ-globulin (158 kDa), ovalbumin (44 kDa), and myoglobin (17 kDa) (Bio-Rad). Calibration curves were constructed by plotting K_{av} *versus* ln (molecular weight), where K_{av} equals $(V_e - V_0)/(V_t - V_0)$. V_e is the measured elution volume of the markers. V_0, the void volume of the column, was determined by gel filtration of blue dextran, and V_t, the total column volume, was specified by the manufacturer (GE Healthcare).

Tryptic Digest—Stocks of trypsin were made from a lyophilized powder (Sigma T-8253) to 10 mg/ml in 1 mM HCl, 20 mM $CaCl_2$, and aliquots were flash-frozen in liquid N_2 and stored at −80 °C. IRF-3 and IRF-3 5E were diluted to 1.25 mg/ml in 80 μl of 25 mM Tris-HCl (pH 8.5), 150 mM NaCl, and 1 mM DTT. Trypsin was diluted to 0.5 mg/ml before use, and the digest was started by adding 1 μl of protease (ratio of protease:substrate was 1:200) to the mix. At each time point trypsin was inactivated with phenylmethylsulfonyl fluoride and EDTA and boiling of the sample for 5 min in SDS loading buffer. The samples were analyzed on a 4–20% gradient SDS-PAGE. For Edman

Downloaded from http://www.jbc.org/ by guest on October 12, 2019

sequencing, the protein was transferred onto polyvinylidene difluoride membrane. Coomassie-stained bands were excised and sequenced at the Tufts University Core Facility (Boston).

Analytical Ultracentrifugation—Samples for analytical ultracentrifugation were dialyzed against 10 mM MOPS (pH 7.5), 150 mM NaCl, and 0.25 mM Tris (2-carboxyethyl)phosphine hydrochloride (TCEP) using a 3500 molecular weight cutoff dialysis membrane (Pierce). The dialysis buffer was used as a blank and as diluent for centrifugation. Analytical centrifugation was performed using an Optima XL-A analytical ultracentrifuge (Beckman Coulter) with an AN-60 Ti rotor. Six-channel cells were used, and data were acquired at a resolution of 0.001 cm with five replicates at a temperature of 4 °C. Absorbance at 280 nm was used to monitor concentration gradients. IRF-3 concentrations were 9, 4.5, and 2 μM, and the speeds were 12,000, 15,000, and 22000 rpm. IRF-3 5E concentrations were 8, 5, and 2 μM, and the concentration distribution was measured at three different rotor speeds, 8,500, 12,000, and 15,000 rpm. Samples were determined to have reached equilibrium when scans taken 4 h apart showed no systematic differences. The protein partial specific volume was calculated from the amino acid composition to 0.7235 ml/g, and solvent density was calculated through summation of the contribution of buffer components to 1.00658 g/cm^3 at 4 °C using the program SEDNTERP (www.cauma.uthscsa.edu/software/). Molecular mass was determined using Beckman software provided as an add-on to Origin version 4.1. All nine data sets were analyzed using a global fit procedure based on a model describing an ideal non-interacting single component system, with local parameters for reference concentrations and base-line offsets and global parameters for the molecular weight. Best-fits were determined through visual inspection of the residuals.

Assessment of Phosphorylation—10-μg aliquots of each protein were desalted by microbore reverse phase liquid chromatography on a 300A polystyrene-divinylbenzene column. Intact protein phosphorylation load was estimated by ESI ion trap (Bruker-Agilent) and by MALDI-TOF mass spectrometry prior to tryptic digestion aided by microwave irradiation (CEM Corp.; 5 min, 50 °C, 25 watts). Individual peptide phosphorylation levels were measured simultaneously by flow injection of the entire desalted tryptic digest and analysis of ESI-FTICR spectra (Bruker 9.4T). The accuracy of this method was confirmed by spiking the tryptic digest with known amounts of two pairs of mono- and diphosphorylated *versus* nonphosphorylated peptides. Phosphorylation sites were deduced by collision-induced dissociation time-of-flight tandem mass spectroscopy (CID TOF MS/MS; AB 4700).

Purification of IBiD and in Vitro Protein Interaction Assay—IBiD was overexpressed in *Escherichia coli* BL21(DE3) with an N-terminal His tag. The protein was purified using nickel-nitrilotriacetic acid resin (Qiagen) followed by reversed-phase high pressure liquid chromatography and verified by electrospray ionization mass spectrometry. ~50 mg of purified IBiD was bound to 1 ml of 50% nickel-nitrilotriacetic acid resin in 20 mM Tris (pH 8.0), 300 mM NaCl, 20 mM imidazole, and excess protein was removed by washing in the same buffer. For each binding reaction 10 μg of each of the different IRF-3 preparations was incubated with 20 μl of IBiD-charged nickel-nitrilotriacetic acid resin in a total volume of 40 μl. The reaction was incubated at 4 °C for 30 min, and a 10-μl sample (input) was removed. The beads were collected by a 1-min centrifugation at 500 × *g*, and a 10-μl sample of the supernatant was taken. The beads were than washed twice with 500 μl of 20 mM Tris (pH 8.0), 300 mM NaCl, 30 mM imidazole, and finally bound protein was eluted by boiling in SDS-loading buffer. The protein samples were resolved on a 4–20% gradient SDS-PAGE.

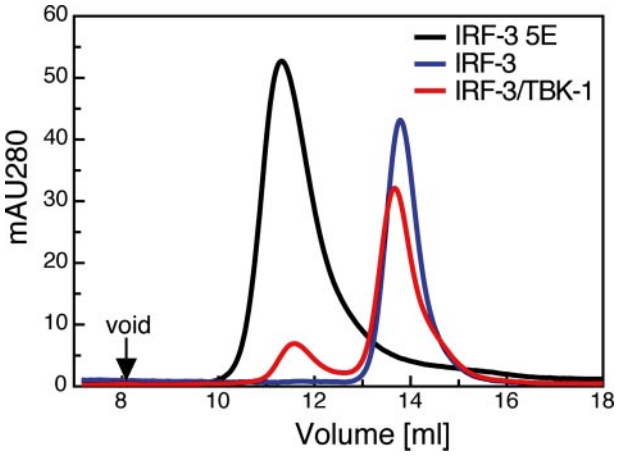

FIGURE 1. **Size exclusion chromatography of purified IRF-3 (*blue*), IRF-3 5E (*black*), and IRF-3 after phosphorylation with TBK1 (*red*).** Phosphorylated IRF-3 elutes in two peaks at 13.6 and 11.6 ml from the gel filtration column.

RESULTS

Purification of IRF-3, IRF-3 5E, IRF-3 2A, and TBK1—FLAG-tagged IRF-3, the constitutively active mutant IRF-3 5E, the mutant IRF-3 2A (T404A/S405A), and the kinase TBK1 were purified from the supernatant of a freeze-thaw lysate of recombinant baculovirus-infected Sf21 cells using a FLAG resin followed by size exclusion chromatography on a Superdex S200 column. This procedure yielded about 0.6 mg of IRF-3 or IRF-3 2A, 0.3 mg of IRF-3 5E, and 0.9 mg of TBK1 per liter of insect cell culture. To analyze the effect of TBK1 phosphorylation on IRF-3 *in vitro*, we incubated TBK1 with IRF-3 or IRF-3 2A and analyzed the products by size exclusion chromatography. IRF-3 has the calculated molecular mass of 48 kDa. As shown in Fig. 1, purified IRF-3 eluted as a single peak with a K_{av} of 0.41, corresponding to an apparent molecular mass of 111 kDa. The mutant IRF-3 5E eluted as a single peak with a K_{av} of 0.24, corresponding to an apparent molecular mass of 316 kDa. When IRF-3 was preincubated with the kinase TBK1, the protein eluted in two peaks from the column. The first peak had a K_{av} of 0.41, the same as unphosphorylated IRF-3, and the second peak had a K_{av} of 0.24, identical to that of IRF-3 5E. SDS-PAGE analysis of the two peaks showed an upward mobility shift in the second peak, indicative of phosphorylation (data not shown). Thus TBK1 phosphorylation of IRF-3 leads to a higher molecular weight species with elution properties similar to those of the constitutively active mutant IRF-3 5E. The mutant IRF-3 2A exhibited identical elution profiles and responsiveness to TBKI phosphorylation as the wild-type protein (data not shown).

Analytical Ultracentrifugation of IRF-3 and IRF-3 5E—We performed sedimentation equilibrium experiments on IRF-3

Downloaded from http://www.jbc.org/ by guest on October 12, 2019

and IRF-3 5E to determine the mass and oligomerization state independently of shape and matrix interactions. Both samples were analyzed at three different starting concentrations and three different rotor speeds. For all nine data sets, absorbance data were monitored at 280 nm and the resulting curves fitted using a nonlinear least-squares algorithm (Fig. 2). For both IRF-3 and IRF-3 5E, the residuals showed random distribution, indicating that the samples contained a single monodisperse species. For IRF-3, the data yielded a molecular mass of 52 ± 2 kDa, close to the calculated molecular mass of 48.2 kDa, showing that IRF-3 is a monomer. For IRF-3 5E, we obtained a molecular mass of 103 ± 2 kDa, about double the mass calculated from the composition. We conclude that IRF-3 5E is a dimer.

Mapping of the TBK1 Phosphorylation Sites—As shown in Fig. 1, TBK1 phosphorylation of IRF-3 results in two species, one of which elutes from a size exclusion chromatography column at the same position as dimeric IRF-3 5E. We concluded that TBK1 phosphorylation induces dimerization of IRF-3 *in vitro*, consistent with earlier findings. Having pure, properly folded, and biochemically homogeneous proteins allowed us to investigate further the role of phosphorylation in IRF-3 activation. We analyzed by mass spectroscopy tryptic peptides from unphosphorylated IRF-3, IRF-3 2A, IRF-3 5E, and TBKI-phosphorylated IRF-3 separated by size exclusion chromatography into the dimeric and monomeric fractions. The constitutively active and dimeric IRF-3 5E was 100% phosphorylated at a site 1 residue (Ser^{385} or Ser^{386}; our data did not allow us to distinguish which serine). That is, site 1 had been phosphorylated by insect cell kinases prior to purification, and the protein had dimerized. This constitutive phosphorylation was observed only in the context of the 5E mutation, and there was no phosphorylation of insect cell-expressed wild-type IRF-3, all of which was monomeric. We do not know the identity of the relevant insect cell kinase. After phosphorylation by TBK1, all IRF-3 had acquired a phosphate at site 2 (Ser^{404} or Thr^{405}; our data did not allow us to distinguish which residue). The IRF-3 that remained monomeric (peak at 13.6 ml in Fig. 1) had not been modified at site 1, whereas the IRF-3 that had dimerized (peak at 11.6 ml in Fig. 1) was fully phosphorylated at both sites 1 and 2. To investigate further the role of phosphorylation at Ser^{404} and Thr^{405}, we mutated these residues to alanine (IRF-3 2A) and repeated the TBK1 kinase assay, gel filtration and phosphate mapping studies. The IRF-3 2A mutant dimerized, and peptide analysis showed that dimerization was dependent on phosphorylation of Ser^{385} or Ser^{386} as in the wild-type protein. In addition, we detected in both monomeric and dimeric TBK1-treated IRF-3 2A a single phosphorylation event in one of the three remaining site 2 positions (serine 396, 398, or 402). These data imply that phosphorylation at site 1 leads to dimerization, as both the TBK1 phosphorylation-dependent dimer and the IRF-3 5E dimer have been phosphorylated there. These data also show that phosphorylation at site 1 occurs only when site 2 bears a negative charge either from phosphorylation or from the 5E mutation. We never found a species that had a phosphate at site 1 without either a phosphate or a phosphomimetic at site 2. Finally, we can conclude that TBK1 phosphorylates preferentially at site 2, as this site was fully phosphoryl-

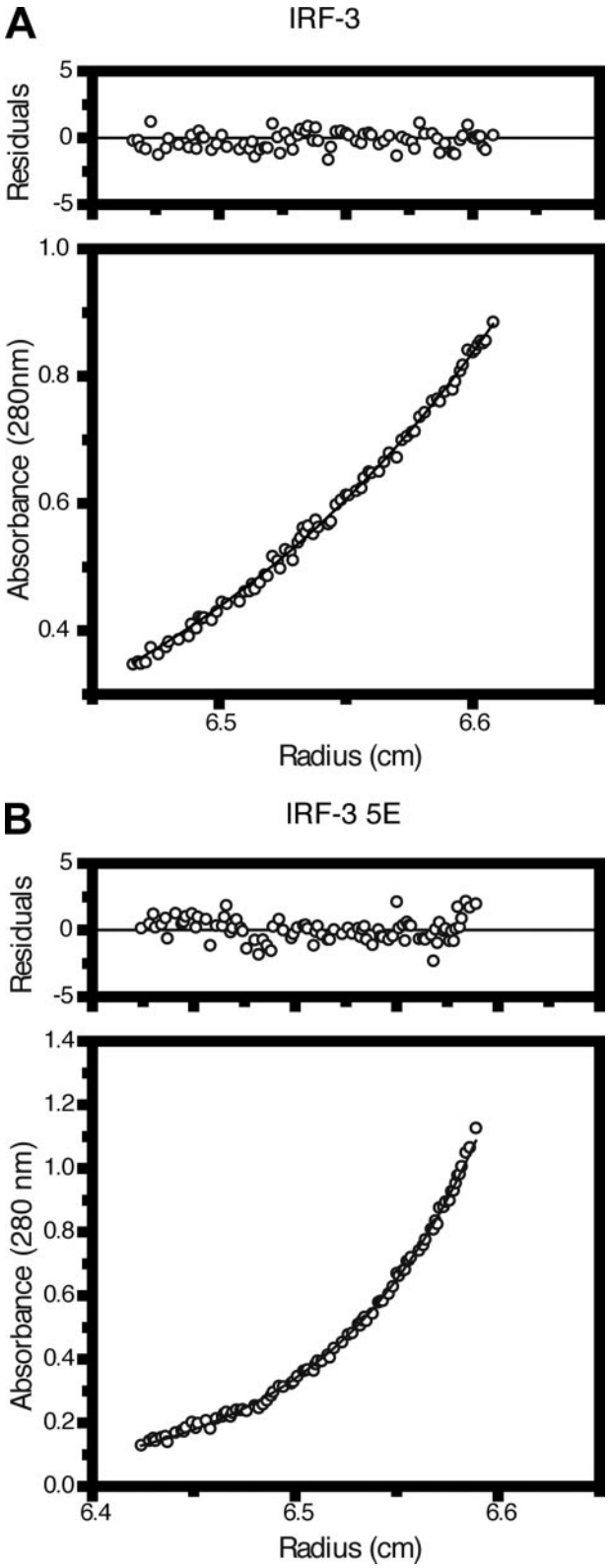

FIGURE 2. **Sedimentation equilibrium analytical ultracentrifugation of IRF-3 and IRF-3 5E.** *A*, shown is the plot of the concentration of 5 μM IRF-3 as a function of the radial distance after reaching equilibrium at 12,000 rpm. The *solid line* is derived from a global fit of all nine data sets to a model describing an ideal non-interacting single-component system. The small random scatter in the residuals indicates that this model describes the data well. *B*, plot as described above for IRF-3 5E at a concentration of 4.5 μM at 12,000 rpm. Note that the concentration distribution curve of IRF-3 5E is steeper than that of IRF-3, indicating the larger mass.

Downloaded from http://www.jbc.org/ by guest on October 12, 2019

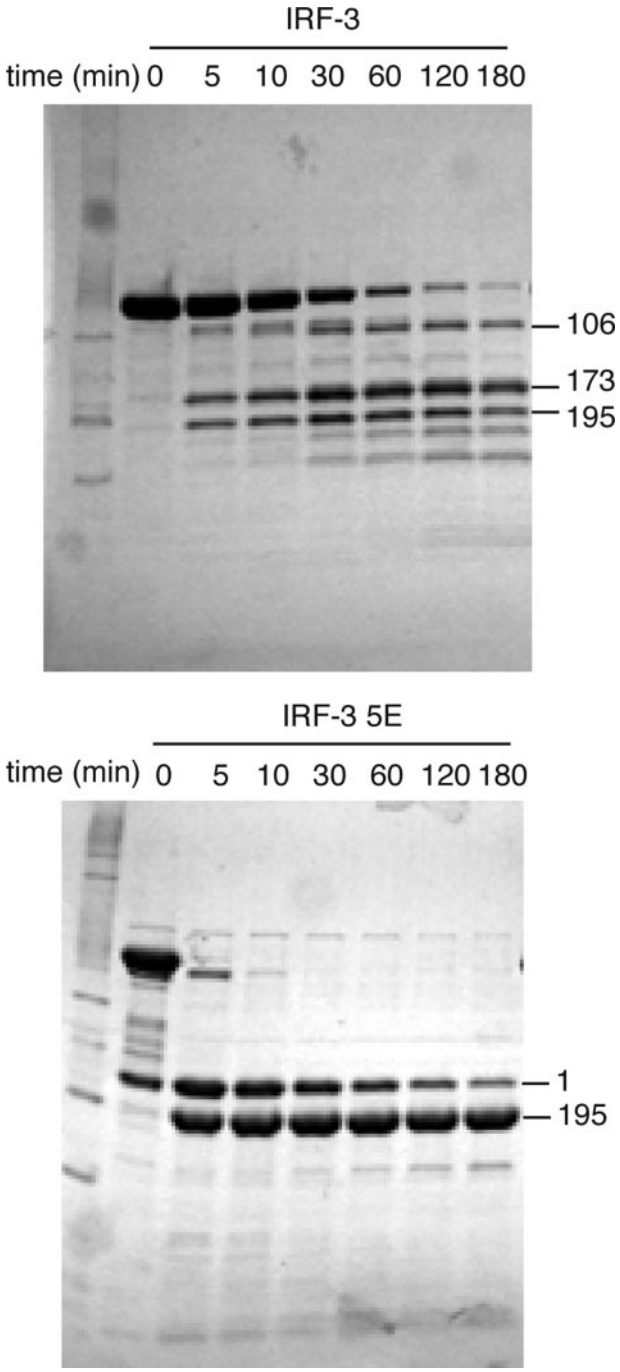

FIGURE 3. **Limited proteolysis of IRF-3 (*top*) and IRF-3 5E (*bottom*).** The samples were incubated at 21 °C for the indicated amount of time. After digestion, trypsin was inactivated with phenylmethylsulfonyl fluoride, EDTA, and boiling of the sample, and the proteins were separated by SDS-PAGE. Cleavage positions as determined by N-terminal amino acid sequencing are shown on the *right*.

ated in both monomer and dimer, whereas only the fraction that had been converted to dimer had a phosphate at site 1 (Fig. 1). Our data indicate that positions in site 2 can be targeted redundantly by TBK1, as mutation of residues 404/405 to Ala did not abolish site 2 phosphorylation.

Trypsin Digestion of IRF-3 and IRF-3 5E—The structures of the C-terminal activation domain of IRF-3 in the presence and absence of the IRF-3-binding domain from CBP have been

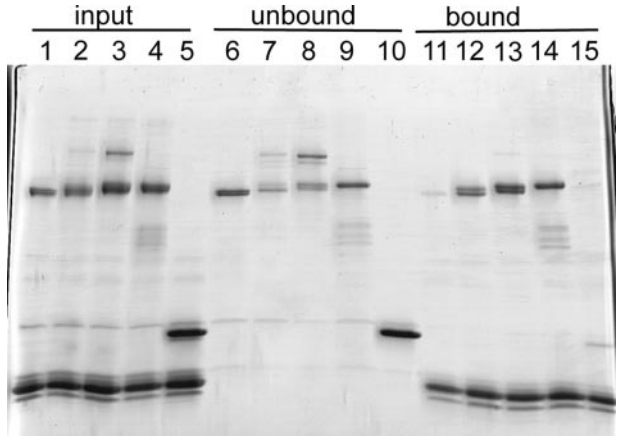

FIGURE 4. ***In vitro* pulldown analysis using immobilized IBiD peptide.** *Lanes 1–5*, respectively: input IRF-3; IRF-3 phosphorylated on Thr^{404}/Ser^{405}; IRF-3 phosphorylated on Thr^{404}/Ser^{405} and Ser^{385}/Ser^{386}; IRF-3 5E; IRF-3 DNA-binding domain. *Lanes 6–10*, unbound protein. *Lanes 11–15*, bound protein.

determined previously (15, 16, 19). They show that the conformations of the latent, autoinhibited IRF-3 and of the IBiD-bound complex are mutually exclusive. The autoinhibitory helices 1 and 5 must be displaced to expose a hydrophobic pocket containing the helices 3 and 4 that interact with the IBiD. Thus we expect that phosphorylation induces structural rearrangements in the domain, which ultimately allow interaction with IBiD and dimerization. We probed monomeric IRF-3 and dimeric IRF-3 5E by limited proteolysis (Fig. 3) and found that IRF-3 5E is more susceptible than wild type to tryptic digestion. After a 10-min incubation, most of the IRF-3 5E had been digested, whereas only a fraction of wild type had been cleaved at that time point. These data show that latent, autoinhibited IRF-3 is less labile than IRF-3 5E dimer. IRF-3 5E cleavage leads to two major products. N-terminal sequencing showed that the larger product derives from the N terminus of the protein and that the smaller product results from cleavage C-terminal to Arg^{194} (N-terminal LLVPGE). Limited proteolysis and mass spectrometry indicated that this fragment was further cleaved at residue 409, resulting in a stable proteolytic fragment comprising amino acids 195–409. Cleavage sites 195 and 409 are within autoinhibitory helices 1 and 5, respectively. In contrast, proteolytic cleavage of wild-type IRF-3 displayed markedly slower kinetics and resulted in three major proteolytic products with N termini at 106, 173, and 195. We conclude that dimeric, activated IRF-3 5E has undergone a large conformational change that involves displacement of helices 1 and 5, allowing efficient protease cleavage at Arg^{194} and Lys^{409}. In the autoinhibited IRF-3 structure, these sites are not readily accessible because of interaction of helices 1 and 5 with helices 3 and 4 (15).

Interaction with CBP—To determine the effect of IRF-3 phosphorylation on the interaction with CBP, we performed pulldown experiments using immobilized IBiD from CBP as bait. As shown in Fig. 4, TBK1-phosphorylated IRF-3 monomer (phosphorylated on site 2) and dimer (phosphorylated on site 1 and site 2) and the constitutive dimer IRF-3 5E (phosphorylated on site 1) all interacted with IBiD, whereas the full-length unphosphorylated IRF-3 or the N-terminal DNA-binding domain of IRF-3 did not. That is, introduction of a negative

Downloaded from http://www.jbc.org/ by guest on October 12, 2019

charge at site 2, either through phosphomimetic mutations (IRF-3 5E) or through TBK1-mediated phosphorylation, is sufficient to alleviate autoinhibition and allow interaction with IBiD. Dimerization, induced by phosphorylation of site 1, was not required for IBiD binding.

DISCUSSION

We present evidence that a dual phosphorylation-dependent switch regulates activation of IRF-3. Phosphorylation of both site 1 and site 2 is required for full IRF-3 activation. Phosphorylation at site 2 is critical for alleviating autoinhibition and allowing interaction with CBP. Phosphorylation at site 1 is in turn essential for IRF-3 dimerization.

TBK1 fully phosphorylated site 2, whereas phosphorylation at site 1 ranged between 20 and 50%, as measured by IRF-3 dimerization. We suggest that *in vitro*, TBK1 phosphorylates IRF-3 by a two-step sequential mechanism, in which site 2 is phosphorylated first. Introduction of negative charge in the site 2 residues leads to structural rearrangement of the autoinhibitory segments, and subsequent phosphorylation of site 1 leads to dimerization (Fig. 5). Although our mass spectrometry data could not distinguish which of the two site 1 residues is phosphorylated, it is likely to be Ser^{386}, based on previous work (17) and our unpublished findings.[4]

Although it is well established that TBK1 activates IRF-3 by direct phosphorylation of the C-terminal residues (8, 21), it remains unclear whether TBK1 is the only kinase required for full IRF-3 phosphorylation at sites 1 and 2 *in vivo*. Whereas phosphorylation at site 2 is virus-inducible, several reports, as well as data presented here, indicate that site 1 can be constitutively phosphorylated in 293T cells or insect cells when phosphomimetic mutations are present in site 2 (16, 17). Therefore, we suggest that alleviation of autoinhibition by TBK1 phosphorylation of site 2 leads to a structure that is then efficiently phosphorylated at site 1 by TBK1 or by another kinase. The requirement of a second kinase would be consistent with the observation that TBK1 alone is not sufficient for full IRF-3 activation by Toll-like receptor 3 *in vivo* and that a second signaling pathway mediated by phophatidylinositol-3 kinase or by protein kinase Cα may be required (22, 23). We have no direct evidence for either of these pathways, however.

We show here that phosphorylation of site 2 by TBK1 results in monomeric IRF-3 that is competent to bind CBP. Thus, relief of autoinhibition, but not dimerization, is necessary and sufficient for interaction with CBP. This result is consistent with the crystal structure of IRF-3 in complex with the IBiD of CBP. Both the crystal structure and analytical ultracentrifugation reveal a 1:1 complex between IRF-3 and CBP (19). A 1:1 complex might not be physiologically relevant, because the predominant species of IRF-3 after virus infection is dimeric. A monomeric IRF-3·CBP complex could, however, interact with other IRFs such as IRF-3 or IRF-7 to form homo- or heterodimeric complexes, as suggested previously (1). Our results are consistent with the observation that a S385A/S386A mutant is dimerization-deficient (16). However, our data apparently contradict coimmunoprecipitation experiments showing that a S385A/S386A or a S386A mutant is unable to bind CBP in a virus-inducible manner (5, 18).[4] These mutants should be dimerization-deficient but should be able to bind CBP after virus-induced phosphorylation of the site 2 residues. It is possible that an IRF-3 monomer binds weakly to CBP *in vivo* and that IRF-3 dimerization through phosphorylation of site 1 stabilizes this complex. We also observed that the phosphorylated IRF-3 dimer binds more strongly to DNA than does the phosphorylated IRF-3 monomer (data not shown), supporting the idea that dimeric IRF complexes are required for high affinity binding to CBP and to DNA *in vivo*.

There is inherent functional redundancy among the different site 2 residues, as demonstrated by the properties of phosphomimetic or alanine mutations. For example, mutation of Ser^{396} or Ser^{398} to Ala greatly reduces the virus inducibility of IRF-3, whereas introduction of phosphomimetic Asp at these residues

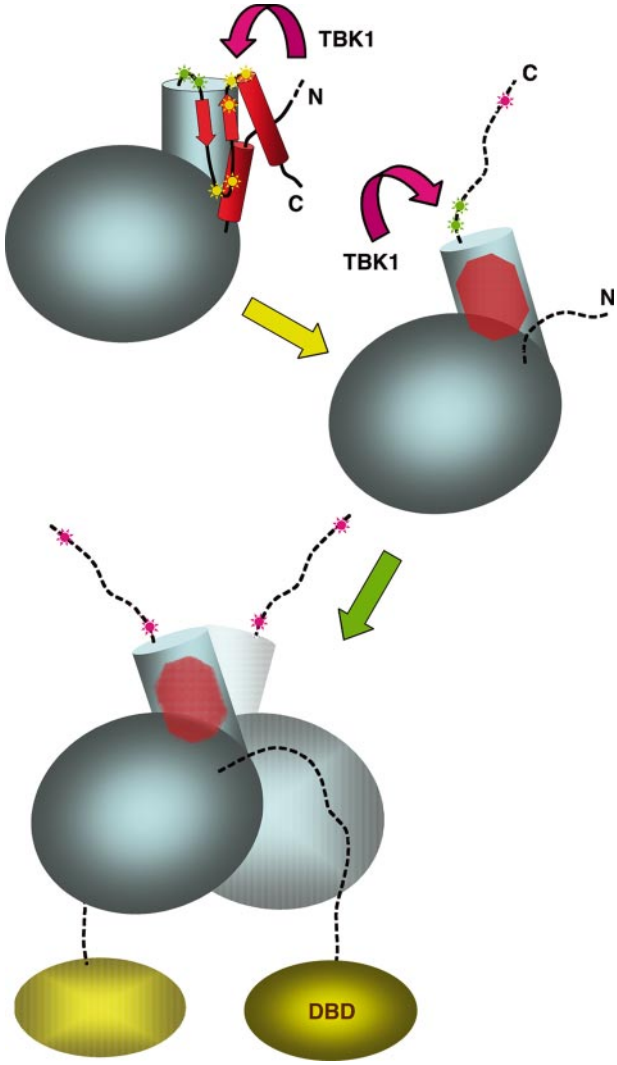

FIGURE 5. **Two-step model of IRF-3 activation by phosphorylation.** The IAD is colored in *blue* and the autoinhibitory structure in *red*. Site 1 phosphorylation sites are labeled with *green stars* and site 2 sites with *yellow stars*. Step 1, the phosphorylation at site 2 by TBK1 alleviates autoinhibition by releasing the autoinhibitory structure, which unfolds after being released (*broken lines*). The phosphorylated residue is labeled in *magenta*. This step unmasks a hydrophobic surface (*red patch*) for interaction with the IBiD of CBP. Step 2, phosphorylation at site 1 (*green stars*) leads to dimerization. The DNA-binding domain is located N-terminally to the IAD.

[4] S. M. McWhirter and T. Maniatis, unpublished observation.

Downloaded from http://www.jbc.org/ by guest on October 12, 2019

is sufficient to generate a constitutive phenotype (11, 18). Similarly, substitution of Ser^{402}, Thr^{404}, or Ser^{405} with Ala reduces virus inducibility, whereas substitution with Asp generates a constitutive phenotype (11, 18). TBK1 phosphorylates an alternative site 2 residue when Thr^{404} and Ser^{405} have been changed to alanine, but our mass spectrometry data do not distinguish which of the three remaining site 2 residues is phosphorylated. The crystal structure of latent IRF-3 has shown that the site 2 residues are part of the autoinhibitory structure and that some of them are partially buried in a hydrophobic environment (15, 16). A plausible activation mechanism, consistent with the structures, is that phosphorylation enforces unfolding of the autoinhibitory elements and consequent exposure of helices 3 and 4 for interaction with the IBiD of CBP (15, 19).

In different cellular contexts, different residues in site 2 appear to be the major targets for activation. Redundancy at site 2 is probably important for a robust and context-independent response, as different signaling pathways will activate different spectra of protein kinases. The identity of the residue within site 2 that is the principal phosphorylation target depends on the specific inducer and cell line used in an experiment, as do the consequences of its modification for phosphorylation of site 1. For example, Ser^{396} is phosphorylated in U373/CD14 astrocytes in response to treatment with Sendai virus and poly(I-C) but not in response to treatment with lipopolysaccharide (18). The IRF 5E variant is active in human 293 cells but much less active in L929 cells (5, 20). These latter observations imply that constitutive phosphorylation of site 1 in the context of the 5E mutation is cell-line dependent, presumably because of different constitutive levels of the relevant kinase activities. We have found in the work described here that the principal residues phosphorylated by TBK1 *in vitro* are Thr^{404} and Ser^{405}. These residues are in the turn between strand β13 and helix α5, part of the hydrophobic core of the autoinhibitory structure (15). Thr 404 forms an N-cap for helix α5 by hydrogen bonding to the backbone amide of Gln^{407}; Ser^{405} has contacts with Lys^{409}, Asp^{406}, and Tyr^{408}. Phosphorylation of either residue 404 or 405 is likely to produce rearrangement of the autoinhibitory structure and unmasking of the hydrophobic surfaces of helices α3 and α4, for interaction with the IBiD of CBP. *In vitro* kinase assays using a glutathione *S*-transferase-fused IRF-3 peptide, residues 380–427, indicate that Ser^{402} is the primary TBK1 target site, but the peptide probably resembles a partially or completely unfolded state of the autoinhibitory region, and it may not represent a principal intracellular conformation. In some cells, phosphorylation of Ser^{396} appears to be the most common modification. Substitution of Ser^{396} with Asp generates a constitutively active form of IRF-3, and mutation to Ala greatly reduces the virus inducibility of IRF-3-regulated genes (18). $Serine^{396}$ is in the loop L6. It forms a hydrogen bond with the main-chain amide of Glu^{201} and potentially with the side-chain of Glu^{200}. We therefore expect that phosphorylation of Ser^{396}, like modification of Thr^{404} or Ser^{405}, will destabilize the autotinhibitory structure (16). In short, the structure of the autoinhibitory region has shown that modification of any of the site 2 residues will trigger the unmasking of the IBiD site and potentiate phosphorylation of site 1; the region appears to have evolved in response to a variety of activating signals and a correspondingly varied spectrum of intracellular responses.

Acknowledgments—We thank Benjamin tenOever of Harvard University for support, David King of the University of California at Berkeley for mass spectrometry, and Michael Berne of the Tufts University Core Facility (Boston) for N-terminal sequencing.

REFERENCES

1. Wathelet, M. G., Lin, C. H., Parekh, B. S., Ronco, L. V., Howley, P. M., and Maniatis, T. (1998) *Mol. Cell* **1,** 507–518
2. Hiscott, J., Pitha, P., Genin, P., Nguyen, H., Heylbroeck, C., Mamane, Y., Algarte, M., and Lin, R. (1999) *J. Interferon Cytokine Res.* **19,** 1–13
3. Genin, P., Algarte, M., Roof, P., Lin, R., and Hiscott, J. (2000) *J. Immunol.* **164,** 5352–5361
4. Barnes, B., Lubyova, B., and Pitha, P. M. (2002) *J. Interferon Cytokine Res.* **22,** 59–71
5. Lin, R., Mamane, Y., and Hiscott, J. (1999) *Mol. Cell. Biol.* **19,** 2465–2474
6. Sharma, S., tenOever, B. R., Grandvaux, N., Zhou, G. P., Lin, R., and Hiscott, J. (2003) *Science* **300,** 1148–1151
7. Fitzgerald, K. A., McWhirter, S. M., Faia, K. L., Rowe, D. C., Latz, E., Golenbock, D. T., Coyle, A. J., Liao, S. M., and Maniatis, T. (2003) *Nat. Immunol.* **4,** 491–496
8. McWhirter, S. M., Fitzgerald, K. A., Rosains, J., Rowe, D. C., Golenbock, D. T., and Maniatis, T. (2004) *Proc. Natl. Acad. Sci. U. S. A.* **101,** 233–238
9. Hemmi, H., Takeuchi, O., Sato, S., Yamamoto, M., Kaisho, T., Sanjo, H., Kawai, T., Hoshino, K., Takeda, K., and Akira, S. (2004) *J. Exp. Med.* **199,** 1641–1650
10. Perry, A. K., Chow, E. K., Goodnough, J. B., Yeh, W. C., and Cheng, G. (2004) *J. Exp. Med.* **199,** 1651–1658
11. Lin, R., Heylbroeck, C., Pitha, P. M., and Hiscott, J. (1998) *Mol. Cell. Biol.* **18,** 2986–2996
12. Yoneyama, M., Suhara, W., Fukuhara, Y., Fukuda, M., Nishida, E., and Fujita, T. (1998) *EMBO J.* **17,** 1087–1095
13. Weaver, B. K., Kumar, K. P., and Reich, N. C. (1998) *Mol. Cell. Biol.* **18,** 1359–1368
14. Panne, D., Maniatis, T., and Harrison, S. C. (2004) *EMBO J.* **23,** 4384–4393
15. Qin, B. Y., Liu, C., Lam, S. S., Srinath, H., Delston, R., Correia, J. J., Derynck, R., and Lin, K. (2003) *Nat. Struct. Biol.* **10,** 913–921
16. Takahasi, K., Suzuki, N. N., Horiuchi, M., Mori, M., Suhara, W., Okabe, Y., Fukuhara, Y., Terasawa, H., Akira, S., Fujita, T., and Inagaki, F. (2003) *Nat. Struct. Biol.* **10,** 922–927
17. Mori, M., Yoneyama, M., Ito, T., Takahashi, K., Inagaki, F., and Fujita, T. (2004) *J. Biol. Chem.* **279,** 9698–9702
18. Servant, M. J., Grandvaux, N., tenOever, B. R., Duguay, D., Lin, R., and Hiscott, J. (2003) *J. Biol. Chem.* **278,** 9441–9447
19. Qin, B. Y., Liu, C., Srinath, H., Lam, S. S., Correia, J. J., Derynck, R., and Lin, K. (2005) *Structure* (*Camb.*) **13,** 1269–1277
20. Suhara, W., Yoneyama, M., Iwamura, T., Yoshimura, S., Tamura, K., Namiki, H., Aimoto, S., and Fujita, T. (2000) *J. Biochem.* (*Tokyo*) **128,** 301–307
21. tenOever, B. R., Sharma, S., Zou, W., Sun, Q., Grandvaux, N., Julkunen, I., Hemmi, H., Yamamoto, M., Akira, S., Yeh, W. C., Lin, R., and Hiscott, J. (2004) *J. Virol.* **78,** 10636–10649
22. Sarkar, S. N., Peters, K. L., Elco, C. P., Sakamoto, S., Pal, S., and Sen, G. C. (2004) *Nat. Struct. Mol. Biol.* **11,** 1060–1067
23. Johnson, J., Albarani, V., Nguyen, M., Goldman, M., Willems, F., and Aksoy, E. (2007) *J. Biol. Chem.*

Downloaded from http://www.jbc.org/ by guest on October 12, 2019

Interferon Regulatory Factor 3 Is Regulated by a Dual Phosphorylation-dependent Switch

Daniel Panne, Sarah M. McWhirter, Tom Maniatis and Stephen C. Harrison

J. Biol. Chem. 2007, 282:22816-22822.
doi: 10.1074/jbc.M703019200 originally published online May 25, 2007

Access the most updated version of this article at doi: 10.1074/jbc.M703019200

Alerts:
- When this article is cited
- When a correction for this article is posted

Click here to choose from all of JBC's e-mail alerts

This article cites 22 references, 13 of which can be accessed free at
http://www.jbc.org/content/282/31/22816.full.html#ref-list-1

Downloaded from http://www.jbc.org/ by guest on October 12, 2019